

“© 2013 IEEE. Personal use of this material is permitted. Permission from IEEE must be obtained for all other uses, in any current or future media, including reprinting/republishing this material for advertising or promotional purposes, creating new collective works, for resale or redistribution to servers or lists, or reuse of any copyrighted component of this work in other works.”

# Medium Frequency-Link Power Conversion for High Power Density Renewable Energy Systems

Md. Rabiul Islam, Youguang Guo, Jianguo Zhu,  
Haiyan Lu

Faculty of Engineering and Information Technology  
University of Technology, Sydney, Australia  
Md.Islam@uts.edu.au, Rabiulbd@hotmail.com

Jianxun Jin

Center of Applied Superconductivity and Electrical  
Engineering  
University of Electronic Science and Technology of China  
Chengdu, China

**Abstract**—Recent advances in solid-state semiconductors and magnetic materials have provided the impetus for medium frequency-link based medium voltage power conversion systems, which would be a possible solution to reducing the weight and volume of renewable power generation systems. To verify this new concept, in this paper, a laboratory prototype of 1.26 kVA medium frequency-link power conversion system is developed for a scaled down 1 kV grid applications. The design and implementation of the prototyping, test platform, and the experimental results are analyzed and discussed. It is expected that the proposed new technology would have a great potential for future renewable and smart grid applications.

**Keywords**—amorphous alloy; medium frequency-link; medium voltage converter; renewable energy systems; direct grid integration

## I. INTRODUCTION

Currently, there are over 282 GW of wind power and over 69 GW photovoltaic (PV) generation capacity installed worldwide and more than 10 MW renewable power plants have now become a reality. The renewable energy source has variable daily and seasonal patterns and consumer power demand requirements also have different characteristics. Therefore, it is difficult to operate a stand-alone power system supplied from only one type of renewable energy resource unless there are appropriate energy storage facilities. If enough energy storage capacity is not available especially in medium/large scale systems a grid connected renewable power generation may be the only practical solution. For grid connection, a power frequency (50 or 60 Hz) step-up transformer is usually used in the renewable generation system to feed the renewable energy into a medium voltage grid (e.g. 6–36 kV). For example, the weight and volume of a 0.69/33 kV, 2.6 MVA transformer are typically in the range of 6–8 tons and 5–9 m<sup>3</sup>, respectively [1]. A liquid-filled 2 MVA step-up transformer uses about 900 kg of liquid as the coolant and insulator, which requires regular monitoring and replacement. This heavy and large size power frequency transformer significantly increases the weight and volume of the system as well as the running and maintenance costs of the renewable generation systems. These drawbacks are critical in offshore and remote area applications, where the costs of installation and regular maintenance are extremely high.

During the last few years, scientists and researchers have been trying to find out effective technologies for the compact and lightweight renewable generation systems. Elimination of step-up transformer by medium voltage converter has attracted

great attention recently. Considering the recent advances in solid-state semiconductors and magnetic materials, the modular multilevel cascaded converter topology may be the natural choice for the development of medium voltage converters [2, 3]. A multi-coil modular permanent magnet generator [4] and a few 6-phase generators [5] were proposed to eliminate the step-up transformer of the wind turbine power generation systems. However, these approaches require special modular generators or multiple traditional generators to generate isolated multiple DC supplies for the modular multilevel cascaded converter, and introduce electrical isolation problem between generator and grid. In order to overcome these drawbacks, a multiphase isolated DC/DC converter based medium voltage PV inverter topology was proposed in [6]. In this system, the voltage balancing is the challenging issue, since each module is connected to a PV array through a DC/DC converter. As an improvement, a single DC-link based PV inverter has been presented in [7]. Although this design may reduce the voltage balancing problem on the grid side, the generation of common DC-link voltage from different PV arrays makes the inverter operation complex and limits the range of operation of the maximum power point tracker (MPPT).

As an alternative approach, a common medium frequency-link based medium voltage converter was reported in [8, 9]. The electromagnetic design and analysis of the medium frequency-link was reported in [10, 11]. This paper presents the overall design and implementation of medium frequency inverter, and fast recovery diode based rectifiers for each module, and test results of the medium frequency-link power conversion system. The medium frequency-link based medium voltage power electronic converter will have the following advantages: (i) having no requirement of special or multiple generators for wind turbine generator systems, (ii) having a wide range of MPPT operation for PV systems, (iii) inheriting the DC-link voltage balance due to single DC supply, (iv) allowing a direct grid connection without using transformers, (v) being an overall compact and lightweight system, and (vi) minimizing inherently the grid isolation problem through medium frequency-link.

The electromagnetic design and analysis of the medium frequency-link was reported in [10, 11]. This paper presents the overall design and implementation of medium frequency inverter, and fast recovery diode based rectifiers for each module, and test results of the medium frequency-link power conversion system. The medium frequency-link based medium voltage power electronic converter will have the following advantages: (i) no requirement of special or multiple generators

for wind turbine generator systems, (ii) wide range of MPPT operation for PV systems, (iii) inherent DC-link voltage balance due to single DC supply, (iv) direct grid connection without using transformer, (v) overall compact and lightweight system, and (vi) inherently minimizing the grid isolation problem through medium frequency-link.

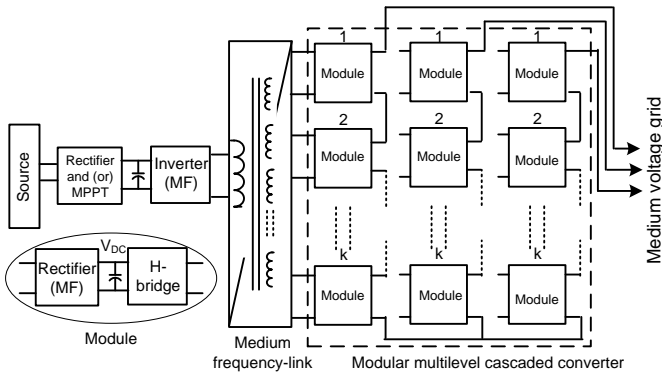


Figure 1. Block diagram of medium frequency-link based medium voltage converter system for step-up transformer-less direct grid connection of renewable power sources.

## II. DESIGN AND IMPLEMENTATION OF MEDIUM FREQUENCY INVERTER

A full-bridge medium frequency inverter is developed by using Semikron SK30GH123 compact insulated gate bipolar transistor (IGBT) module. This inverter can generate a square wave primary excitation voltage of the medium-frequency-link with a medium frequency. The Semikron SKHI 20opA with SKHI PS1 is used as an isolated driver for SK30GH123 module. Fig. 1 shows a photograph of the medium-frequency inverter. A high speed PWM controller UC3825BN is used to generate the switching signals. A simplified version of the switching signal generator circuit is shown in Fig. 2. UC3825BN is a high performance PWM controller with low start up current, accurate oscillator frequency, leading edge blanking, latched fault logic, full-cycle soft start, restart delay after fault and many more.

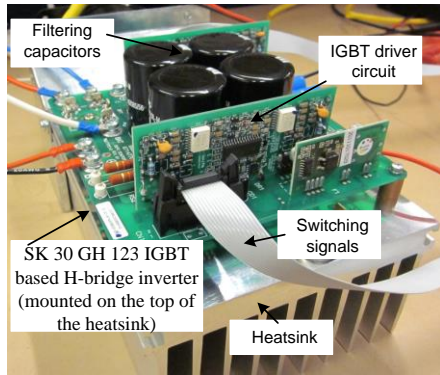


Figure 2. A photo of medium-frequency inverter

The oscillator of the UC3825BN is a saw-tooth which utilizes two pins; one for the timing resistor  $R_T$  and the other for timing capacitor  $C_T$ . The resistor programs the charging

current to the timing capacitor via an internal current mirror with high accuracy. Maximum signal high time is determined by the rising capacitor voltage whereas dead time is determined by the timing capacitor discharge.

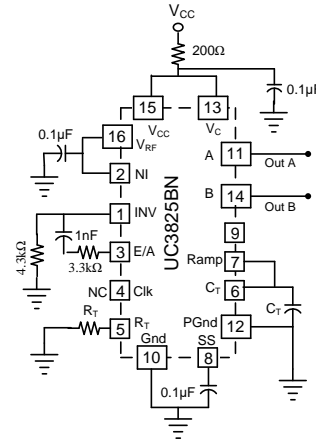


Figure 3. Simplified circuit of the switching signal generator.

Based on the desired maximum duty cycle,  $D_{max}$ , the timing resistor can be calculated as

$$R_T = \frac{3V}{10mA \times (1 - D_{max})} \quad (1)$$

$$= \frac{3V}{10mA \times (1 - 0.90)} = 3 \times 10^3 \Omega = 3k\Omega.$$

Two alternative signals are generated through a T flip-flop; output signal frequency is the half of oscillator frequency as configured internally. Therefore, twice oscillator frequency (compare to output) is required to design the timing capacitor. Based on the calculated value of timing resistor and desired maximum duty cycle the timing capacitor can be calculated as

$$C_T = \frac{1.6 \times D_{max}}{R_T \times f} \quad (2)$$

$$= \frac{1.6 \times 0.90}{3 \times 10^3 \times 20 \times 10^3} = 2.4 \times 10^{-8} F = 24nF.$$

The complete switching signal generator circuit with UC3825BN IC is fabricated and tested in the Laboratory. The gate pulses were measured and compared with the simulation results as shown in Fig. 4. The measured pulses were found highly consistent with the simulation results.

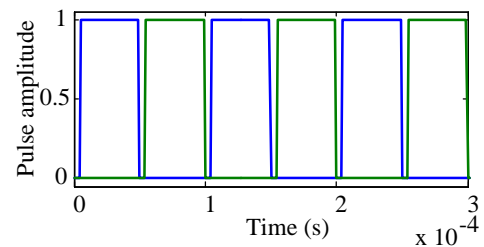


Figure 4. Simulated gate pulses to drive the medium frequency inverter. In Matlab simulation environment 1 V gate pulses are capable to drive the IGBTs.

The signal high time (switch on) and dead time (switch off) are measured using cursors of the oscilloscope as shown in Figs. 5 and 6 and duty cycle is also calculated.

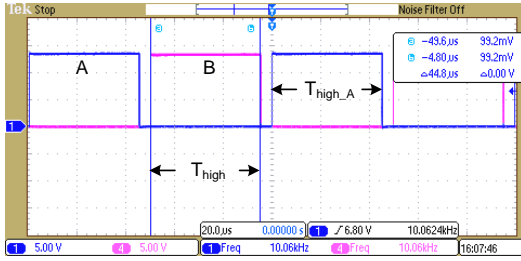


Figure 5. Measured switching signals; on-time calculation

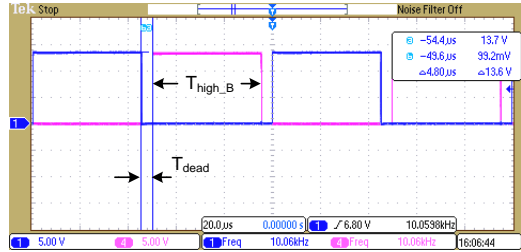


Figure 6. Measured switching signals; dead-time calculation

The percentage of duty cycle,  $D\%$  can be calculated as

$$D\% = \frac{T_{high}}{T_{high} + T_{dead}} \times 100 \quad (3)$$

$$= \frac{44.8}{44.8 + 4.8} \times 100 = 90.30\% .$$

The expected time period,  $T$  and frequency,  $f_H$  of the medium frequency inverter can also be calculated as

$$T = T_{high\_A} + T_{dead\_A} + T_{high\_B} + T_{dead\_B} \quad (4)$$

$$= 44.8\mu s + 4.8\mu s + 44.8\mu s + 4.8\mu s = 99.2\mu s .$$

$$\therefore f_H = \frac{1}{T} = \frac{1}{99.2 \times 10^{-6}} = 10.08kHz .$$

### III. DESIGN AND IMPLEMENTATION OF MEDIUM FREQUENCY RECTIFIERS

Single phase diode rectifier is considered to convert medium frequency alternating quantity to DC quantity with fast recovery diodes. Each module is associated with a separate rectifier. The available average voltage is about 367 V. Table I depicts the technical information of the module rectifier.

TABLE I. POWER COMPONENTS IN THE INVERTER SIDE RECTIFIER

Technical data	Value
Unit voltage (rms)	375 V
Average output voltage	367 V
PIV of the diodes	375 V

The input voltage waveform of this rectifier is like alternating train of pulses. The rectified output waveform can

be compared with DC/DC chopper circuit output. The IXYS DSEE15-12CC super fast recovery (25 ns) dual diode module is considered for the development of module rectifier of medium voltage converter. If we assume the capacitor discharge rate to remain constant at the DC level, the peak to peak ripple voltage,  $V_{r(p-p)}$  can be approximated by a waveform as shown in Fig. 7, which has a peak to peak value of  $\Delta V_o$  and a time period of  $T_r$  and centered around the DC level.

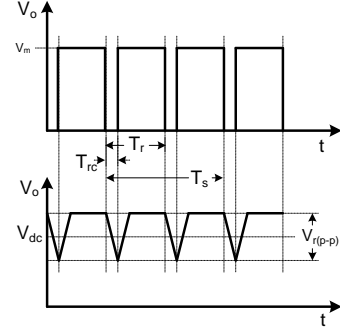


Figure 7. Capacitor voltage of the module rectifier

If  $I_{dc}$  is the output rectifier average current,  $f_s$  is the source voltage frequency,  $V_{dc}$  is the output rectifier DC output voltage,  $D_{off}$  is the diode off time or capacitor discharge time factor, and  $\gamma$  is the ripple factor, then the peak to peak and rms output voltage can be deduced as

$$V_{r(p-p)} = \frac{I_{dc} D_{off} T_r}{C} = \frac{I_{dc} D_{off}}{C f_r} = \frac{I_{dc} D_{off}}{2 C f_s} \quad (5)$$

$$\text{and } V_{r(rms)} = \frac{V_{r(p-p)}}{2\sqrt{3}} = \frac{I_{dc} D_{off}}{4\sqrt{3} C f_s} \quad (6)$$

Hence, the ripple factor can be deduced as

$$\gamma = \frac{V_{r(rms)}}{V_{dc}} = \frac{I_{dc} D_{off}}{4\sqrt{3} C f_s V_{dc}} \quad (7)$$

From (7), minimum value of the capacitor can be deduced as

$$C = \frac{I_{dc} D_{off}}{4\sqrt{3} \gamma f_s V_{dc}} F \quad (8)$$

If  $I_{dc}$  is 1 A,  $f_s$  is 10 kHz,  $V_{dc}$  is 367 V,  $D_{off}$  is 2% and ripple factor is 1%, the minimum value of capacitor,  $C$  for the each module rectifier can be calculated as

$$C = \frac{1 \times 0.02}{4\sqrt{3} \times 0.01 \times 10 \times 10^3 \times 367} = 78.66nF .$$

The 3188EE152T400APA1 aluminum electrolytic capacitor is used for the module rectifier circuit. The maximum power handled by a power diode and the temperature of the diode junction are related since the power dissipated by the device causes an increase in temperature at the junction of the device. The junction temperature ( $T_J$ ), case temperature ( $T_C$ ), and ambient (air) temperature ( $T_A$ ) are related by the device heat-handling capacity can be presented in terms of thermal-electric analogy as

$$\theta_{JA} = (\theta_{JC} + \theta_{CS} + \theta_{SA}) \quad (9)$$

and

$$T_J = P_D \theta_{JA} + T_A, \quad (10)$$

where  $\theta_{JA}$  is the total thermal resistance (junction to ambient),  $\theta_{JC}$  is the transistor thermal resistance (junction to case),  $\theta_{CS}$  is the insulator thermal resistance (case to heat sink),  $\theta_{SA}$  is the heat-sink thermal resistance (heat sink to ambient), and  $P_D$  is the power dissipation. Using (9) and (10) the heat-sink thermal resistance can be deduced as

$$\theta_{JC} + \theta_{CS} + \theta_{SA} = \frac{T_J - T_A}{P_D}$$

$$\theta_{SA} = \frac{T_J - T_A}{P_D} - (\theta_{JC} + \theta_{CS}). \quad (11)$$

From the data sheet of DSEE15-12CC,  $\theta_{JC}$  is 1.60 °C/W,  $\theta_{CS}$  is 0.5 °C/W,  $T_J$  is 170 °C and  $P_D$  is about 2 W. Therefore, the heat-sink thermal resistance can be calculated as

$$\theta_{SA} = \frac{170 - 40}{2} - (1.6 + 0.5) = 62.9^\circ C/W.$$

#### IV. EXPERIMENTAL TESTING AND RESULTS ANALYSIS

A scaled down prototype of 1.26 kVA medium frequency-link with single primary and six secondary windings is developed, as shown in Fig. 8 to generate the balanced isolated six DC supplies for a three-phase five-level modular multilevel cascaded converter. Fig. 9 shows the voltage waveform of primary and secondary sides of the medium frequency-link. An Agilent Technologies DS06034A oscilloscope with P5200 high voltage differential probe was used to observe the voltage waveform. The measured waveforms were found highly consistent with the theoretical and simulation results. The simulated primary and secondary sides voltage waveforms are shown in Figs. 10 and 11.

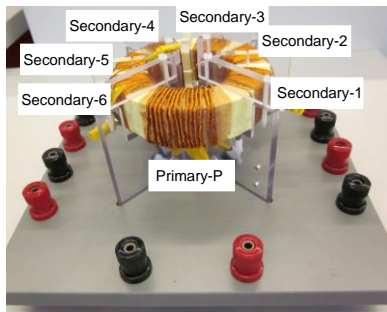


Figure 8. A photo of the medium frequency-link; single primary and 6 secondary windings; Metglas 2605SA1 sheet of 20  $\mu$ m thickness and 25 mm width was glued with Araldite 2011 on the surface of each layer to develop the core. To minimize the proximity effect, Litz wires are used for windings with single layer placement.

The DC-link voltages were measured and found approximately equal at about 367 V. Fig. 12 shows the measured voltage waveform of the medium frequency rectifier, which is found highly consistent with simulation results. The Fig. 13 shows the simulated voltage waveform of rectifier circuit. The B-H curves of the medium frequency-link

were analyzed at different magnitudes of excitation currents and at different excitation frequencies. The plotted B-H curves have been compared with the material manufacturer's data and found highly consistent. Fig. 14 shows the B-H curves at excitation currents of 12 kHz. The developed medium frequency-link power conversion system is tested with a three-phase five-level 1 kV modular multilevel cascaded converter and found highly satisfactory performance. The line voltages of the modular multilevel cascaded converter after filter circuit are shown in Fig. 15.

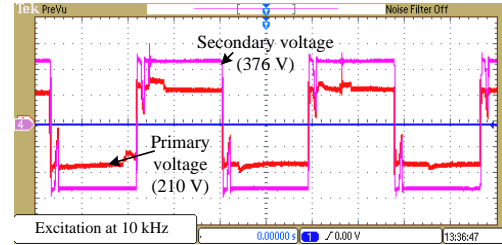


Figure 9. Measured primary and secondary side voltages of the prototype medium frequency-link.

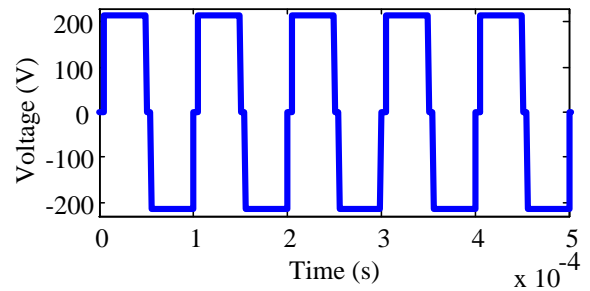


Figure 10. Simulated primary side voltage of the medium frequency-link; at 10 kHz excitation current.

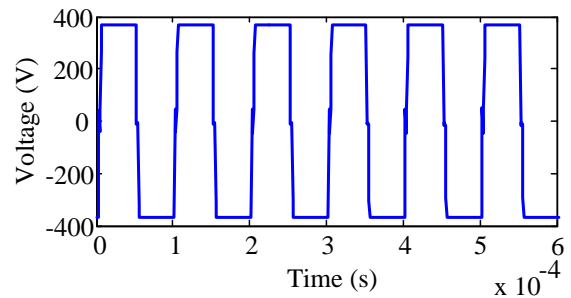


Figure 11. Simulated secondary side voltage of the medium frequency-link; at 10 kHz excitation current.

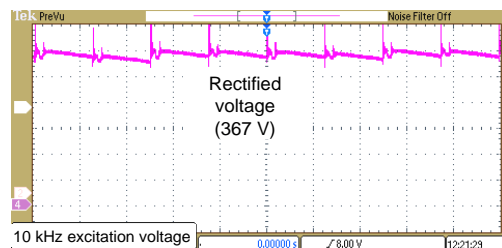


Figure 12. Measured rectified output voltage of the prototype medium frequency rectifier.

The measured line voltages of the proposed system were also compared with the simulation results, and they were found highly consistent with the theoretical and simulation results. Fig. 16 shows the simulated line voltages of the 1 kV converter system after line filter.

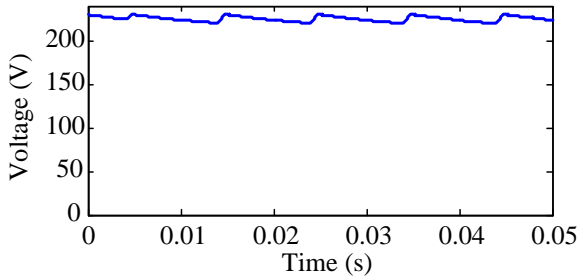


Figure 13. Simulated output voltage of the medium frequency rectifier.

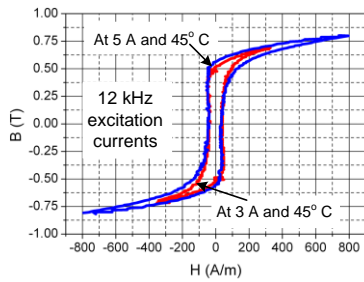


Figure 14. Measured B-H curves at excitation currents of 3 A and 5 A. The link is excited by 12 kHz square wave primary voltage. The magnetic field intensity and magnetic flux density are calculated by measuring the primary-coil excitation current and open circuit terminal voltage of each of the six secondary coils.

## V. CONCLUSION

The proposed medium frequency-link can be a good solution to provide balanced isolated multiple DC supplies for modular multilevel cascaded converter to develop medium voltage converter. This medium voltage converter based direct grid connection approach eliminates not only the grid side heavy transformer but also reduces the size of line filters.

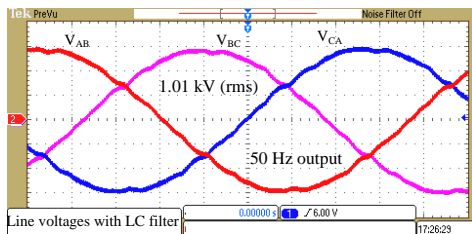


Figure 15. Measured line voltages of the prototype 1 kV converter.

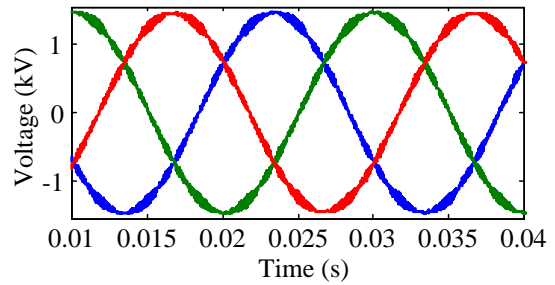


Figure 16. Simulated line voltages of the proposed 1 kV converter.

## REFERENCES

- [1] M. R. Islam, Y. G. Guo, and J. G. Zhu, "A transformer-less compact and light wind turbine generating system for offshore wind farms," Proc. 2012 IEEE International Conference on Power and Energy, Kota Kinabalu, Malaysia, Dec. 2–5, 2012, pp. 605–610.
- [2] M. R. Islam, Y. G. Guo, J. G. Zhu, and D. G. Dorrell, "Design and comparison of 11 kV multilevel voltage source converters for local grid based renewable energy systems," Proc. 37th Annual Conference of the IEEE Industrial Electronics Society, 7–10 Nov. 2011, Melbourne, Australia, pp. 3596–3601.
- [3] M. R. Islam, Y. G. Guo, and J. G. Zhu, "Performance and cost comparison of NPC, FC and SCHB multilevel converter topologies for high-voltage applications," Prof. Int. Conference on Electrical Machines and Systems, 20–23 Aug. 2011, Beijing, China, pp. 1–6.
- [4] X. Yuan, J. Chai, and Y. Li, "A transformer-less high-power converter for large permanent magnet wind generator systems," IEEE Trans. Sustainable Energy, vol. 3, no. 3, pp. 318–329, July 2012.
- [5] X. Yuan, Y. Li, J. Chai, and M. Ma, "A modular direct-drive permanent magnet wind generator system eliminating the grid-side transformer," Proc. the 13th European Conf. on Power Electronics and Appl., Barcelona, pp. 1–7, Sep. 2009.
- [6] H. Choi, W. Zhao, M. Ciobotaru, V. G. Agelidis, "Large-scale PV system based on the multiphase isolated DC/DC converter," Proc. IEEE International Symposium on Power Electronics for Distributed Generation Systems, Aalborg, Denmark, 25–28 June 2012, pp. 801–807.
- [7] S. Kouro, C. Fuentes, M. Perez, and J. Rodriguez, "Single DC-link cascaded H-bridge multilevel multistring photovoltaic energy conversion system with inherent balanced operation," Proc. 38th Annual Conference on IEEE Industrial Electronics Society, Montreal, QC, Canada, 25–28 Oct. 2012, pp. 4998–5005.
- [8] M. R. Islam, Y. G. Guo, and J. G. Zhu, "A novel medium-voltage converter system for compact and light wind turbine generators," Proc. Australasian Universities Power Engineering Conference, Bali, Indonesia, September 26–29, 2012, pp. 1–6.
- [9] M. R. Islam, Y. G. Guo, and J. G. Zhu, "H-bridge multilevel voltage source converter for direct grid connection of renewable energy systems," Proc. IEEE Power & Energy Society Innovative Smart Grid Technology Conf., 13–16 Nov. 2011, Perth, Australia, pp. 1–7.
- [10] M. R. Islam, Y. G. Guo, and J. G. Zhu, "A medium-frequency transformer with multiple secondary windings for grid connection through H-bridge voltage source converters," Proc. Int. Conf. Ele. Machines and Systems, Sapporo, Japan, Oct. 21–24, 2012, pp. 1–6.
- [11] M. R. Islam, Y. G. Guo, and J. G. Zhu, "A medium-frequency transformer with multiple secondary windings for medium-voltage converter based wind turbine generating systems," Journal of Applied Physics, vol. 113, no. 17, pp. 17A324–17A324-3, May 2013.